# Thickness dependent spin to charge interconversion efficiency in polycrystalline BiSb layers deposited on Si substrate

*Talluri Manoj[1$], Venkat Mattela[2$], Akshay Kumar Salimath[2$], Sanghamitra Debroy[2$], Tarun Raju Kakinada[1], M S Devapriya [3], Arabinda Haldar[3], Zhenchao Wen[4], Hiroaki Sukegawa[4], Seiji Mitani[4], and Chandrasekhar Murapaka[1*]*

[1]Department of Materials Science and Metallurgical Engineering, Indian Institute of Technology Hyderabad, 502284, Telangana, India

[2]Ceremorphic, Inc., San Jose, California 95131, United States of America

[3]Department of Physics, Indian Institute of Technology Hyderabad, 502284, Telangana, India

[4]National Institute for Materials Science, Tsukuba 305-0047, Japan.

[$]Contributed equally to the work

*Corresponding author email: mchandrasekhar@msme.iith.ac.in

# ABSTRACT

The strong spin-orbit torque (SOT) generated by topological insulators (TIs) interfaced with ferromagnetic layers paves the path towards the low-power, high-speed spintronic device applications. To date, large charge-spin or spin-charge conversion efficiency (ξ) of TIs are accomplished on high-quality epitaxially grown TI thin films on specifically oriented substrates. Here, we report the sputtering growth of polycrystalline BiSb on industrially adaptable Si substrate, preserving the topological surface states (TSS) in BiSb. We have performed spin pumping and inverse spin Hall effect (ISHE) measurements on BiSb($x$)/Ti($y$)/Py(10 nm) stacks by varying the thicknesses of BiSb and Ti insertion layer (IL). The ξ has improved from 8 nm to 12 nm of BiSb, and we found ξ of 3.27 in the BiSb(12 nm)/Ti(3 nm)/Py(10 nm) sample. This increasing trend in ξ with the thickness of BiSb is also consistently observed in spin-torque ferromagnetic resonance (ST-FMR) measurements. The improvement in ξ is attributed to the improved stability of TSS in BiSb when the thickness increased from 8 to 12 nm. The Ti IL thickness dependence of ξ study has shown that a 3 nm Ti layer has successfully achieved a trade-off to hinder the interdiffusion between BiSb and NiFe and promote the efficient spin current transport, highlighting the critical role of IL thickness. Our results demonstrate the process involved in depositing a homogeneous BiSb layer directly on the Si substrate and the impact of the thickness of the IL and BiSb on the ξ in topological insulator/ferromagnet bilayer systems.

**Keywords:** Topological insulators, Spin-orbit torques, Polycrystalline BiSb, spin-charge interconversion, Inverse spin Hall effect, Spin-torque ferromagnetic resonance.

# I. INTRODUCTION

A digital world that continuously generates data from various sources, its processing and storage require high density, high speed, long endurance and low power non-volatile memories. Despite rapid advancements in data storage technology leading to increased memory density, the field of spintronics has also made remarkable progress over the past few decades, both fundamentally and technologically. Magnetic Random Access Memory (MRAM) is emerging as a promising candidate as embedded non-volatile memory. Spin-transfer torque (STT) based MRAM is commercially available but for niche applications. However, STT-MRAM has several issues, such as large current densities required for switching and shared read/write paths, posing challenges for realizing memory with high endurance and high speed. Consequently, recent attention has shifted towards spin torques induced by spin-orbit coupling (SOC) in heavy-metal/ferromagnet interfaces.[1–3] An in-plane charge current flowing through a material with large SOC can generate pure spin current in the transverse direction, which exerts spin-orbit torques on the adjacent ferromagnetic layer. Spin-orbit torque (SOT) induced switching offers several advantages over spin transfer torque switching, such as decoupled read/write path current scalability, which can lead to quasi-infinite endurance and high speed. However, SOT switching is currently limited by the low spin-to-charge conversion efficiencies in well-known heavy metal layers.[4–6]The emergence of topological insulators (TIs) presents an extraordinary opportunity to explore novel spin-orbit torque-driven mechanisms.[7] Previous room temperature measurements have shown that TIs like $Bi_2Se_3$, BiSn, BiTe, and BiSb exhibit spin-charge conversion efficiencies several orders of magnitude higher than those observed at transition-metal interfaces.[8–10]However, the widespread application of TIs in MRAM is limited by non-complementary metal-oxide semiconductor (CMOS)-compatible and expensive processing stages required to achieve high-quality ferromagnet/TI interfaces. Among the various TIs, BiSb, a three-dimensional topological insulator with a small bulk band gap, has recently garnered significant attention due to its large spin torque efficiency and high conductivity.[11,12] In molecular beam epitaxy grown samples on GaAs substrate, the charge to spin (spin to charge) conversion efficiency ($\xi$) is observed as high as 52.[11] Recent studies have reported a $\xi$ of 1.2 for sputter-deposited BiSb grown on sapphire substrate.[13] Though there are several attempts to demonstrate the efficient spin-orbit torques in BiSb, it is important to grow these layers using the sputtering technique on a Si substrate to bring them close to practical applications.[14] The low melting point of these materials often leads to island-type growth, resulting in films with relatively large roughness.

It is also important to control the composition of BiSb to observe the topological surface states (TSS). Therefore, the optimization of sputtering growth of BiSb with the right composition and low roughness on Si substrate is of great interest. The low melting point of TIs also leads to the interdiffusion at the interface between BiSb and ferromagnetic layer, deteriorating the ξ.[15–18], [19] To prevent the interdiffusion, insertion of a low SOC insertion layer has shown significant improvement in ξ. The thickness of the insertion layer plays a vital role in spin current transport between the TI and ferromagnet.[13,20] Therefore, it is of paramount importance to investigate the importance of the thickness of the insertion layer and the BiSb layer on ξ.

In this study, we have successfully sputter-deposited smooth polycrystalline BiSb thin films directly on Si substrates. Stacks of BiSb($x$)/Ti($y$)/Py(10 nm) are prepared by varying the thicknesses of BiSb and Ti insertion layer (IL) to investigate the effect of BiSb and Ti thicknesses on the ξ. We have established the effect of thickness on ξ via ISHE and ST-FMR techniques. Both measurements indicate that the ξ improves with increasing thickness of BiSb. This is due to the stable TSS at higher thickness of BiSb. The Ti layer dependence of ξ shows higher spin transport when the Ti thickness is 3 nm.

# II. METHODS

BiSb is deposited on Si (100) substrate using DC magnetron sputtering. The substrates are cleaned with acetone, IPA, and DI water prior to the deposition. The base pressure and deposition pressure are maintained at $5 \times 10^{-7}$ mbar and $2 \times 10^{-3}$ mbar, respectively. The BiSb target is pre-sputtered for 15 minutes prior to the deposition for conditioning, and the deposition rate of BiSb at the optimized deposition condition is 0.38 nm/s. The composition analysis is carried out using energy-dispersive X-ray spectroscopy (EDS). Ti and $Ni_{81}Fe_{19}$ (Py) are deposited similarly using DC magnetron sputtering at a deposition rate of 0.023 nm/s and 0.16 nm/s, respectively. All depositions are performed at room temperature. A Bruker-made D8 Discover GIXRD system is used for structural characterization. The resistivity measurements are conducted using the four-probe method. We have used a broadband ferromagnetic resonance setup with a coplanar wave guide for spin-pumping and inverse spin Hall effect (ISHE) measurements. The Keithley-2182 nano-voltmeter is used to measure the ISHE voltage. For ST-FMR measurements, the microwires are patterned from the multilayers using UV lithography and ion milling techniques. Coplanar waveguide devices made of sputter-deposited Ta (10)/Au (100) were prepared using conventional UV lithography and the lift-off method.

# III. RESULTS AND DISCUSSION

## (a) BiSb growth and characterization

The deposition of BiSb thin film on a Si(001) substrate from a single $Bi_{85}Sb_{15}$ alloy target is carried out using DC magnetron sputtering. We have optimized the deposition parameters to achieve a composition of $Bi_{83}Sb_{17}$, which is confirmed by the energy dispersive spectroscopy (EDS). Fig. 1 (a) shows the roughness of the BiSb (10 nm) film, and the rms roughness is confirmed to be ~ 0.33 nm from the atomic force microscopy (AFM) measurements. It is observed that the roughness of the films has increased drastically for the thickness greater than 14 nm (Supplementary information Fig. S1). Four-probe resistivity measurements were conducted for BiSb films with thicknesses 4, 5, 6, 8, 10, 12, 14, 16, and 18 nm to understand the topologically insulating nature of the BiSb films. The resistivity data at different thicknesses of BiSb is shown in Fig. 1(b). Barua et al. have shown the thickness dependence of resistivity of TIs, where the resistivity of the film is high at the lower thickness,

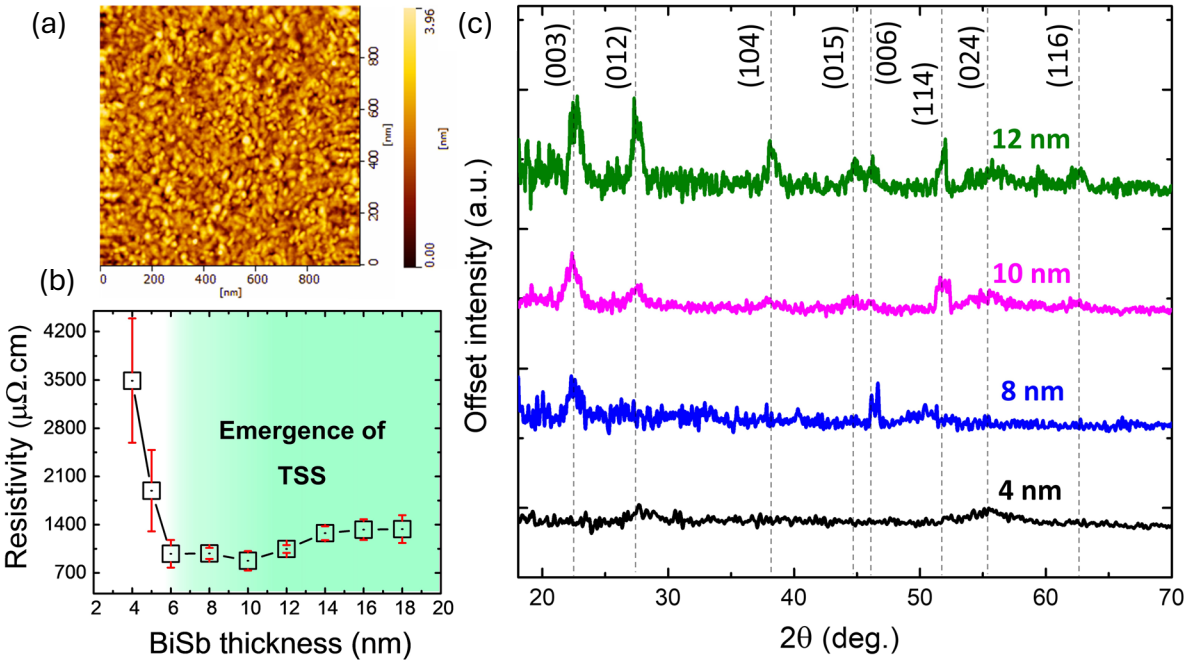


Fig. 1. *(a) AFM topography image of BiSb (10 nm) sample with rms roughness of 0.33 nm, (b) Resistivity of BiSb films at different thicknesses showing the presence of TSS, ( XRD plots of 4 nm, 8 nm, 10 nm and 12 nm BiSb showing polycrystalline nature of the films grown on Si substrates.*

then decreases with increasing thickness, and after a critical thickness, it increases again with the thickness of TIs.[21] A systematic measurement of roughness is carried out on the samples with different thicknesses of BiSb. The AFM micrographs and the estimated roughness values are shown in the supplementary information in Fig. S2 and S3, respectively. The resistivity of the 10 nm BiSb film is in the range reported in the literature.[13] Structural characterization is performed using grazing incidence X-ray diffraction (GIXRD). Fig. 1 (c) show the XRD plots of BiSb of 4, 8, 10, and 12 nm thickness. The films are observed to be polycrystalline in nature with the presence of both (003) and (012) orientations. It is to be noted that (012) orientation has started to appear in the BiSb films with thicknesses of 10 and 12 nm. The importance of the crystal structure of BiSb on the ξ is highlighted in the literature.[14,22] However, achieving a specific orientation such as (012), or (003) becomes impractical considering the complexity involved in depositing such epitaxial films. In such a scenario, achieving polycrystalline films on Si substrate becomes viable. Here, we have systematically investigated the effect of the thickness variation of the polycrystalline BiSb and Ti insertion layer on spin-to-charge conversion. We have prepared a total of six stacks of BiSb/Ti/Py deposited to understand the effect of BiSb and Ti layer thickness on the spin-to-charge conversion efficiency (ξ) through inverse spin Hall effect (ISHE) measurements. A Si (sub.)//BiSb (10)/Ti (0 nm)/Py (10 nm) stack is prepared as a reference sample and named as A1. The stacks Si (sub.)//BiSb (*x*)/Ti (3 nm)/Py (10 nm) where *x* = 8, 10, 12 nm are named as A2, A3, and A4, and the stacks Si (sub.)//BiSb (10 nm)/Ti (*x*)/Py (10 nm)/cap where x = 4, 8 nm named B1, B2.

## (b) Spin-to-charge conversion efficiency (ξ) estimation from Inverse spin Hall effect measurements

The schematic for the ferromagnetic resonance (FMR) based spin-pumping and ISHE measurements in the trilayer stack is shown in Fig. 2(a). In spin-pumping, an RF field perturbs the magnetization of Py and drives it into precession when the FMR condition is satisfied. The precessing magnetization of the Py layer loses angular momentum at the interface and injects pure spin current into the BiSb layer through the Ti insertion layer, and the high SOC in the surface states of the BiSb layer creates a non-equilibrium charge accumulation due to ISHE or inverse Rashba Edelstein effect. A nano-voltmeter was employed to measure the charge accumulation. Figures 2 (b) and (c) show the measured FMR signal and the corresponding ISHE voltage ($V_{meas}$) as a function of the external magnetic field ($H_{ext}$) at an excitation frequency ($f$) of 9 GHz. The symmetric ($V_{sym}$) and antisymmetric ($V_{asym}$) voltage components

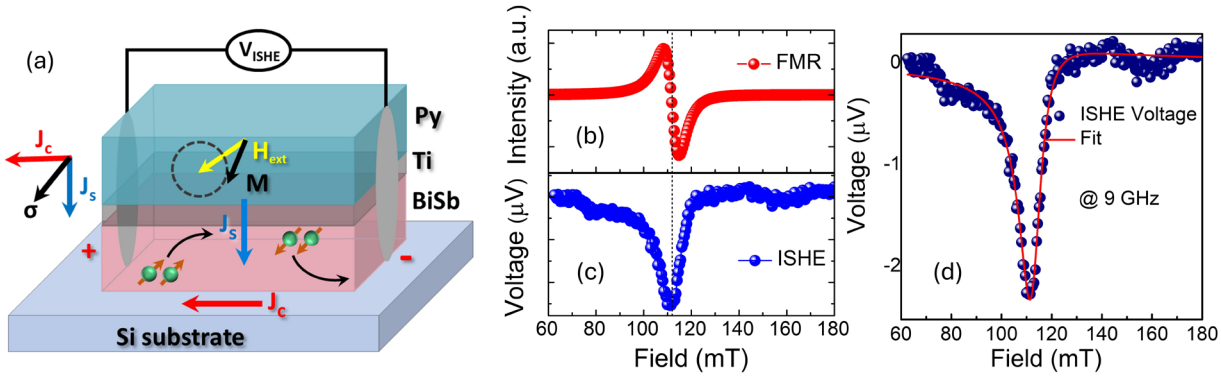


Fig. 2. *(a) Schematic of the FMR and ISHE phenomena showing the magnetization (M), spin current flow ($J_s$), and charge current ($J_c$); (b), (c) FMR response and the ISHE voltage of the sample A3-Si (sub.)//BiSb (10 nm)/Ti (3 nm)/Py (10 nm)/cap at 9 GHz, respectively showing the high ISHE voltage at the FMR resonance field; (d) ISHE volage and the fit to equation (1) to extract $V_{sym}$, $V_{asym}$*

of the obtained ISHE voltage signal are extracted by fitting the signal to equation (1), as shown in Fig. 2(d).

$$V_{\text{meas}} = V_{\text{sym}} \frac{(\Delta H)^2}{(H-H_{\text{res}})^2+(\Delta H)^2} + V_{asym} \frac{2\Delta H(H-H_{\text{res}})}{(H-H_{\text{res}})^2+(\Delta H)^2} \qquad (1)$$

Here, $\Delta H$ is the linewidth, and $H_{\text{ext}}$ is the external DC magnetic field. The damping constant ($\alpha$) values were obtained from equation (2) by fitting the $\Delta H$ vs $f$.

$$\Delta H = \Delta H_0 + \frac{4\pi\alpha f}{\gamma} \qquad (2)$$

Where $\Delta H_0$ corresponds to the inhomogeneous linewidth broadening. The values of $\Delta H_0$ observed in our samples are less than 1.5 mT, which indicates the homogeneity of our samples.

Angular ISHE measurements are performed where the sample with contacts is rotated in 360° with respect to the magnetic field direction. These angular measurements help in extracting the voltage generated due to spin pumping ($V_{\text{sp}}$) and the other rectification effects, such as anomalous Hall voltage ($V_{\text{AHE}}$) and anisotropic magnetoresistance ($V_{\text{AMR}}$) from the angular dependence on $V_{\text{sym}}$. The experimental data of $V_{\text{sym}}$ vs angle (between the field and the sample) and the fit to equation (3) for the sample A3 are shown in Fig. 3 (a).

$$V_{\text{sym}} = V_{\text{sp}}\cos^3(\varphi+\varphi_0) + V_{\text{AHE}}\cos(\varphi+\varphi_0)\cos\varphi \qquad (3)$$

$$+V_{\text{sym}}^{\text{AMR}}\cos 2(\varphi+\varphi_0)\cos(\varphi+\varphi_0)$$

$$+V_{\text{sym}}^{\text{AMR}}\sin 2(\varphi_0)\cos(\varphi+\varphi_0)$$

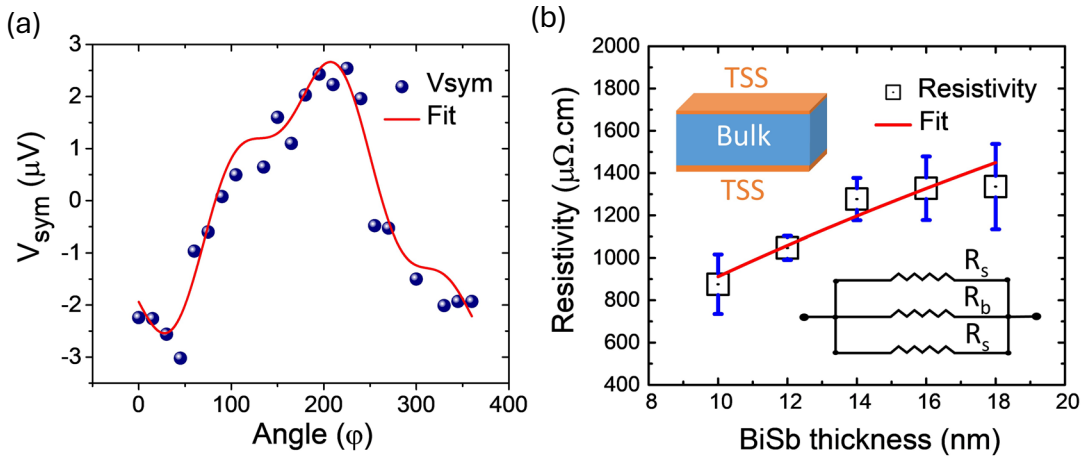


*Fig. 3. (a) $V_{sym}$ data of sample A3 measured at the field in 360 degrees in the in-plane direction, and the solid line is the fit to equation (3), (b) Thickness dependence resistivity in the metal-like region (10 to 18 nm), and the solid line is fit to equation (6). The inset shows the representative schematic of TSS and bulk states and the parallel resistance model to estimate the resistance of bulk and TSS.*

Spin mixing conductance ($g_{\text{eff}}^{\uparrow\downarrow}$), a parameter that indicates the spin transparency of the interface of BiSb and Py is extracted using equation (4) where $\alpha_o$ is the bulk damping of Py, i.e, estimated to be 0.008 from FMR measurements.

$$g_{\text{eff}}^{\uparrow\downarrow} = \frac{(\alpha_{\text{eff}} - \alpha_o)\mu_o M_s t_{\text{FM}}}{g\mu_o\mu_B} \tag{4}$$

The spin current density ($J_s$) in BiSb is estimated using the equation (5). The value indicates a spin transport across the interfacial layer from Py to BiSb. The resistivity of the films (ρ) measured at different thicknesses ($t$) is used to estimate the resistivity of the surface states ($\rho_s$) and the bulk ($\rho_b$) using the parallel resistor model. A region in which the resistivity increases with the thickness is chosen to fit with Equation 6 to extract both bulk and TSS resistivities, as shown in Fig. 3 (b). The resistivity of the TSS is used to further estimate the ξ.

The spin current to charge current conversion efficiency (ξ) is estimated by using equation (7).[23] Where $W$ is the width of the signal line of the CPW. In the case of the topological insulators, the spin current injected from FM is converted to a charge current within the length of the TSS due to their high SOC strength. This means that the spin diffusion length ($\lambda_s$) will be equal to the length of the TSS, i.e., $t_{\text{NM}} = \lambda_s$. The modified equation (8) is used to estimate the ξ of the sample.

$$J_s = \left(\frac{g_{\uparrow\downarrow}\hbar}{8\pi}\right)\left(\frac{\mu_o h_{\text{rf}}\gamma}{\alpha_{\text{eff}}}\right)^2 \left[\frac{\mu_o M_s\gamma + \sqrt{(\mu_o M_s\gamma)^2 + 16(\pi f)^2}}{(\mu_o M_s\gamma)^2 + 16(\pi f)^2}\right]\left(\frac{2e}{\hbar}\right) \tag{5}$$

$$\rho = \frac{\rho_s\rho_b t}{2\rho_b t_s + \rho_s(t - 2t_s)} \tag{6}$$

The ξ is given as:

$$\xi = \frac{V_{sp} \cdot \left(\frac{t_{Py}}{\rho_{Py}} + \frac{t_{Ti}}{\rho_{Ti}} + \frac{t_{BiSb}}{\rho_{BiSb}}\right)}{W.\lambda_s.\tanh\left(\frac{t_{NM}}{2\lambda_s}\right).J_s} \quad (7)$$

$$\xi = \frac{V_{sp} \cdot \left(\frac{t_{Py}}{\rho_{Py}} + \frac{t_{Ti}}{\rho_{Ti}} + \frac{t_{BiSb}}{\rho_{BiSb}}\right)}{W.\lambda_s.\tanh\left(\frac{1}{2}\right).J_s} \quad (8)$$

The ξ of the samples, A1, A2, A3, and A4, were found to be 0.7, 1.49, 2.46, and 3.27, respectively, while considering the $\lambda_s$ as 2 nm.[24] The spin pumping voltage, spin mixing conductance, and spin current densities are also reported in Table 1. The magnetic field angular dependence of $V_{sym}$ for samples A1, A2, A4, B1, and B2 is shown in Supplementary information, Fig. S4. Similarly, the ξ is estimated for B1 and B2 where the Ti insertion layer thickness is changed, and the results are shown in Table 2.

Table 1: Spin pumping voltage, spin mixing conductance, spin diffusion length, and the ξ of the samples A1, A2, A3 and A4 estimated from spin pumping and ISHE measurements

| **Sample** | **Spin-pumping voltage, $V_{sp}$ (μV)** | **Spin mixing conductance ($m^{-2}$) ×$10^{18}$** | **Spin current density ($A/m^{-2}$) ×$10^5$** | **Spin diffusion length (nm)** | ξ |
|---|---|---|---|---|---|
| A1-BiSb(10)/Ti(0)/Py(10)/cap | 1.69 ± 0.6 | 3.88 | 1.37 | 2 | 0.7 |
| A2-BiSb(8)/Ti(3)/Py(10)/cap | 2.77 ± 0.3 | 3.41 | 1.47 | 2 | 1.49 |
| A3-BiSb(10)/Ti(3)/Py(10)/cap | 5.27 ± 0.5 | 3.00 | 1.46 | 2 | 2.46 |
| A4-BiSb(12)/Ti(3)/Py(10)/cap | 8.14 ± 0.3 | 2.71 | 1.49 | 2 | 3.27 |

The comparison between A1 and A2 shows that the insertion of a Ti layer significantly enhanced the spin Hall angle. This demonstrates the importance of the Ti layer as an IL.[13] It was observed that with the increase in the thickness of the BiSb, in A2, A3, and A4, the ξ values increased. This enhanced spin Hall angle could be due to the improved stability of the TSS with the increase in BiSb thickness. To get an insight into the effect of the Ti insertion layer thickness on the ξ, we have varied Ti IL thickness. The spin-pumping and ISHE results are summarized in Table 2. As the thickness of the Ti layer increases from 4 nm to 8 nm, a decrease in both the spin pumping voltage and the system's ξ is observed. It is to be noted that the spin mixing conductance and the spin current density are slightly different for samples A1, A2, A3,

and A4. This means that the change in damping and spin mixing conductance depends on the adjacent layers (Ti or BiSb) to the spin source layer Py.

The actual quantity of spin current reaching BiSb from Py could be less than expected due to the scattering of spin current and spin memory loss within the Ti layer. With a higher thickness of the spacer layer, the scattering of the spin current in Ti increases, thus reducing the amount of spin current reaching the Ti/BiSb interface. This justifies the reduction in ξ when the thickness of Ti increases. This experiment highlights the importance of choosing the optimum thickness of an insertion layer. Though the spin Hall angle is reduced with increasing insertion layer thickness, it is still higher than 1 and much higher than the conventional heavy metal-based spin Hall layers.[25–28] We have plotted the dependence of Ti and BiSb thickness on the spin current density and ξ to demonstrate the trend clearly in supplementary information in Fig. S5 (a) and (b).

Table 2: Spin pumping voltage, spin mixing conductance, spin diffusion length, and the ξ of the samples B1 and B2 with Ti insertion layer of 4 nm and 8 nm, respectively.

| Samples | Spin-pumping voltage, $V_{sp}$ (μV) | Spin mixing conductance ($m^{-2}$) ×$10^{18}$ | Spin current density ($A/m^{-2}$) ×$10^{5}$ | Spin diffusion length (nm) | ξ |
|---|---|---|---|---|---|
| B1-BiSb(10)/Ti(4)/Py(10)/cap | 3.96 ± 1.1 | 2.55 | 1.47 | 2 | 1.91 |
| B2-BiSb(10)/Ti(8)/Py(10)/cap | 2.7 ± 0.9 | 2.67 | 1.44 | 2 | 1.53 |

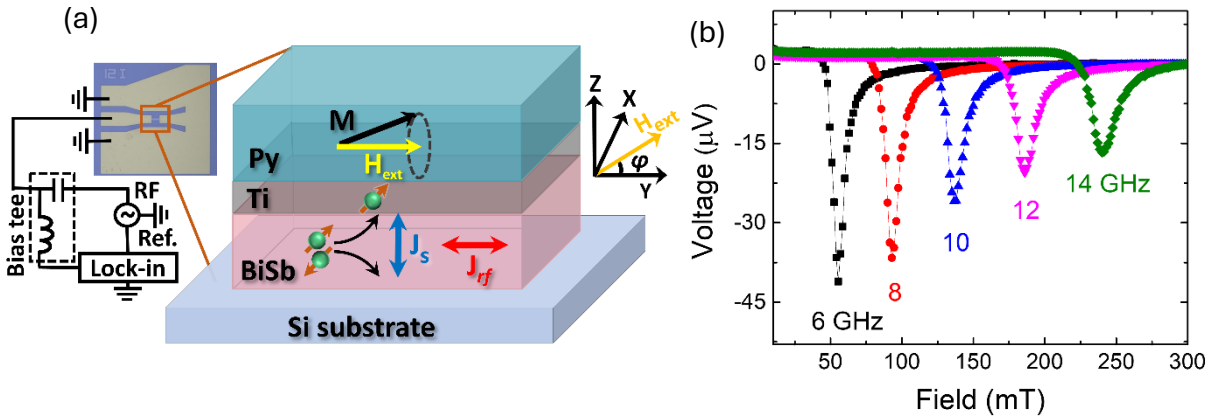


*Fig. 4. (a) Schematic representation of the spin transport from BiSb to Py through Ti and the ST-FMR setup (b) ST-FMR response of the sample A3.*

## (c) Charge to spin conversion efficiency (ξ) estimation from ST-FMR measurements

In order to further confirm the thickness dependence of BiSb on ξ, spin torque ferromagnetic resonance (ST-FMR) measurements are performed on the samples A2, A3 and A4. The ST-FMR setup consists of a microwave source to inject RF current into the CPW device using the GSG probe, and a lock-in amplifier to detect the DC voltage as shown in the schematic Fig. 4(a). An external magnetic field was applied in-plane and swept in the range of 0 to 300 mT while a microwave current passed through the CPW, inducing the precession of the magnetic moments in the ferromagnetic layer. The spin current generated because of the spin Hall effect or the interfacial Rashba effect in the topological insulator layer travels towards Py and exerts torque on its magnetization.[29,30] This interaction results in a measurable voltage signal (mixing voltage) due to AMR in Py. The measured AMR signals obtained at various RF frequencies (6-14 GHz) as a function of the magnetic field. The ST-FMR data for the sample A3 is shown in Fig. 4(b). The measured voltage as a function of the applied magnetic field was analysed to extract the resonance field and linewidth. The symmetric and antisymmetric components of the voltage signal are separated to determine the contributions from the spin Hall effect and Oersted field, respectively. Linewidth ($\Delta H$), resonance field ($H_{\mathrm{res}}$), and symmetric ($S$) and antisymmetric ($A$) voltage signals were extracted by fitting the ST-FMR spectra to the equation (9).

$$V_{\mathrm{mix}} = S\frac{\Delta H^2}{\Delta H^2+(H_{\mathrm{ext}}-H_{\mathrm{res}})^2} + A\,\frac{\Delta H(H_{\mathrm{ext}}-H_{\mathrm{res}})}{\Delta H^2+(H_{\mathrm{ext}}-H_{\mathrm{res}})^2} \tag{9}$$

$$\xi = \frac{S}{A}\frac{e\mu_{\mathrm{o}}M_{\mathrm{s}}d_{\mathrm{BiSb}}t_{\mathrm{Py}}}{\hbar}\left(1+\frac{\rho_{BiSb}}{\rho_{Ti}}.\frac{t_{Ti}}{t_{BiSb}}\right)\sqrt{1+\frac{4\pi M_{\mathrm{eff}}}{H_{\mathrm{o}}}} \tag{10}$$

The change in symmetric (S) and asymmetric (A) components as a function of in-plane angular magnetic field for the samples A2, A3 and A4 are shown in the Supplementary Information, Fig. S6. Both S and A are observed to be following the form of $\sin(2\varphi)\cos(\varphi)$ as shown in the literature.[13] The ξ is estimated by using equation (10) and the values are found to be 1.80, 2.22 and 2.61 for the samples A2, A3 and A4, respectively. The ST-FMR results further confirm the thickness dependence of the ξ of BiSb layer. In accordance with the ISHE results, the ξ is improved as the BiSb thickness is increased from 8 to 12 nm. We have limited our studies to 12 nm of BiSb, considering the increased roughness with increasing thickness of BiSb due to the grain growth in the out-of-plane direction at higher thickness of BiSb, which is detrimental to the spin current transport at the interface and ξ. The increasing trend observed in the spin-to-charge and charge-to-spin conversion efficiencies from our results highlights the role of BiSb thickness. The improvement of ξ with BiSb might be due to the dominant bulk contribution or the isolation of topological surface states. Chi *et al.* have argued that the spin

Hall conductivity of BiSb is predominantly contributed by bulk as compared to the topological surface states.[15] Therefore, with higher BiSb thickness, the relative thickness of the bulk increases and its contribution to the ξ increases before it saturates. Furthermore, as the BiSb thickness is increased, the surface states become more isolated, reducing overlap and hybridization, thereby enhancing the spin-momentum locking effect and increasing ξ. Khang *et al.* have also highlighted the role of the thickness of polycrystalline BiSb on the spin Hall angle and achieved ξ of 3.2 for 10 nm thick polycrystalline BiSb.[31] Fan *et al.* reported ξ of 10.7 for a 10 nm thick polycrystalline BiSb.[32] Both works highlighted the importance of choosing 10 nm BiSb to achieve stable TSS. Table 3 shows the summary from the literature on the spin-charge interconversion efficiency (ξ) reported for the polycrystalline BiSb estimated using various methods. It should be noted that the BiSb is deposited on various buffer layers in the listed works, due to the difficulty in growing flat films directly on the substrate.

Table 3: ξ of polycrystalline BiSb reported in the literature on various substrates and growth techniques.

| **Substrate and underlayer** | **Deposition method of BiSb** | ξ | ξ **estimation method** |
|---|---|---|---|
| $Si/SiO_2$//Ta/BiSb/CFB | MBE | 1.2 | Harmonic Hall[15] |
| $Si/SiO_2$//MgO/[Co/Pt]n/BiSb | Sputtering | 2.4 | Harmonic Hall[12] |
| $Si/SiO_2$//[Co/Tb]n/BiSb | MBE | 3.2 | Harmonic Hall[31] |
| $Al_2O_3$//[Co/Pt]n/BiSb | Sputtering | 10.7 | Harmonic Hall[32] |
| GaAs//(seed)/(Ga,Fe)Sb/BiSb | Co-sputtering | 2.1-2.6 | ISHE[23] |
| Si//BiSb/Ti/NiFe (This work) *Without under layer | Sputtering | 3.27 & 2.61 | ISHE & ST-FMR respectively |

In this work, we addressed the challenge by depositing smooth polycrystalline BiSb films directly on Si substrates using DC magnetron sputtering. This approach enables compatibility with CMOS integration and reduces the complexity that might come from the buffer layers. To prevent intermixing between the BiSb film and the top NiFe layer, we introduced a thin Ti interlayer. Titanium was specifically chosen because, unlike nickel or iron, it does not exhibit miscibility within the BiSb matrix, thereby preserving the structural and functional integrity of the BiSb layer. Further, we have shown that increasing the BiSb thickness up to 12 nm can improve the ξ. From the observations, we conclude that the increase in the ξ, as determined from the ISHE measurements, indicates a significant contribution from the TSS. The spin current injected via spin pumping interacts with the TSS, characterized by

its high SOC strength, and is efficiently converted into charge current. The charge-to-spin conversion in the BiSb layer could be due to contributions from both the TSS and the bulk states in BiSb. As the thickness increases, the electrons interact with both the TSS and the bulk states, influencing the charge-to-spin conversion process. Moreover, the crystallite/grain size estimated for the BiSb films with thicknesses of 8, 10, 12 and 18 nm suggests that the grain size increases with the thickness of BiSb (shown in Supplementary information, Table S1). Le et.al, performed the grain size analysis for the BiSb layer in highly textured or epitaxial films and established a relation between the grain size and the spin Hall angle.[33] As discussed earlier, the (012) orientation of BiSb is observed in 10 and 12 nm films. These combined effects of increased grain size and the presence of (012) orientation could contribute to the enhancement in $\xi$ with increasing thickness of BiSb. While both the ISHE and ST-FMR measurements show an increasing trend in the $\xi$ with the thickness of BiSb, the absolute $\xi$ values differ between the two techniques. One should note that the ISHE measurements we performed are more global, meaning the voltage drop we observe is averaged over the whole area of the sample. Meanwhile, the ST-FMR measurements are local since we patterned the samples into wires. The lower $\xi$ values observed in the ST-FMR measurements could be attributed to the fact that the total current in the BiSb film splits between the TSS and the bulk. Because the SOC strength differs between TSS and the bulk, the overall efficiency of charge-to-spin conversion decreases in ST-FMR measurements. In contrast, ISHE measurements primarily reflect the spin-to-charge conversion occurring in the TSS, resulting in higher $\xi$ values. One of the other minor possibilities for the anomaly is the contact resistance between these two different methods.

The IL improved the interface quality between the topological insulator and the ferromagnetic layer, enhancing the effective spin current transmission at an optimal IL thickness, i.e., 3 nm. Ruixian et.al have reported the importance of the thickness of Ti IL to achieve higher $\xi$.[20] Insertion layers can act as barriers to prevent intermixing or diffusion of atoms between the topological insulator and the ferromagnetic layer, which is particularly important for the device fabrication in the back-end of the line (BEOL) CMOS integration and for device operation at elevated temperatures. The optimal insertion layer thickness ensures effective prevention of intermixing without significantly increasing the distance over which spin currents must travel, which could lead to spin relaxation. This study highlights the importance of choosing the right thickness of the spin Hall layer and the insertion layer to enhance $\xi$ in TI/IL/FM systems. We thus have demonstrated the sputtered growth of the BiSb on Si substrates with relatively high spin Hall efficiencies that will result in easier incorporation into CMOS devices that can be exploited for their use in SOT-based MRAM devices.

# IV. SUMMARY

We have demonstrated the growth of BiSb films with low roughness on Si substrate at room temperature using a magnetron sputtering process, ensuring easier integration into industry-standard CMOS devices. We studied the effect of the thickness of the BiSb layer and the Ti insertion layer on the ξ of the BiSb/Ti/Py heterostructures. The ξ was obtained from ISHE measurements, and it was observed that it is increasing with the thickness of BiSb from 8 to 12 nm in Si (sub.)//BiSb(*x*)/Ti(3 nm)/Py(10 nm)/cap stack. The ξ deteriorates with an increase in Ti layer thickness. A large ξ, i.e., ξ = 3.27, is observed at an optimized thickness of BiSb (12 nm) and Ti (3 nm), in the stack Si (sub.)//BiSb(12)/Ti(3)/Py(10)/cap, which is one order magnitude larger than that of heavy metals. This is due to the TSS in 12 nm BiSb, with 3 nm Ti acting as a barrier to block the interdiffusion of Bi/Sb and Ni atoms. We have also shown that ξ is not limited by the quality of BiSb itself but by the interface between BiSb, Ti, and Py, where Ti preserves the topological surface states of BiSb, enhancing the ξ. ST-FMR measurements are in good agreement with the trend of this increasing ξ with BiSb thickness. The high ξ enables efficient interconversion between spin to charge, which enables its use in SOT-MRAM.

## ACKNOWLEDGMENTS

We thank Mr. Rohiteswar Mondal for the assistance with SEM-EDS measurements. CM would like to thank JICA Friendship 2.0 funding for the support.

## AUTHOR DECLARATIONS

### Conflict of Interest

The authors have no conflicts to disclose**.**

### Author Contributions

VM, AKS and SD conceived the idea of a spintronic device. CM and TM have planned the growth experiments for the stacks and measurements. TM performed all the experiments. TRK, DMS and AH have helped with spin-pumping measurements and analysis. ZW, HS and SM have helped with ST-FMR measurements and analysis. CM has supervised all the experiments. All the authors have discussed and contributed to the manuscript writing.

## DATA AVAILABILITY

Data will be available on request to the corresponding author

## REFERENCES


[1] M.H. Nguyen, and C.F. Pai, "Spin-orbit torque characterization in a nutshell," APL Mater. **9**(3), (2021).

[2] A. Manchon, and A. Belabbes, *Spin-Orbitronics at Transition Metal Interfaces*, 1st ed. (Elsevier Inc., 2017).

[3] L. Liu, C.F. Pai, Y. Li, H.W. Tseng, D.C. Ralph, and R.A. Buhrman, "Spin-torque switching with the giant spin hall effect of tantalum," Science **336**(6081), 555–558 (2012).

[4] M. Kharbouche-Harrari, R. Alhalabi, J. Postel-Pellerin, R. Wacquez, D. Aboulkassimi, E. Nowak, I.L. Prejbeanu, G. Prenat, and G.D. Pendina, "MRAM: from STT to SOT, for security and memory," Proc. - 33rd Conf. Des. Circuits Integr. Syst. DCIS 2018, 1–6 (2019).

[5] G. Prenat, K. Jabeur, P. Vanhauwaert, G. Di Pendina, F. Oboril, R. Bishnoi, M. Ebrahimi, N. Lamard, O. Boulle, K. Garello, J. Langer, B. Ocker, M.C. Cyrille, P. Gambardella, M. Tahoori, and G. Gaudin, "Ultra-Fast and High-Reliability SOT-MRAM: From Cache Replacement to Normally-Off Computing," IEEE Trans. Multi-Scale Comput. Syst. **2**(1), 49–60 (2016).

[6] G. Prenat, K. Jabeur, G. Di Pendina, O. Boulle, and G. Gaudin, "Beyond STT-MRAM, Spin Orbit Torque RAM SOT-MRAM for High Speed and High Reliability Applications," Spintron.-Based Comput., 1–253 (2015).

[7] J. Han, and L. Liu, "Topological insulators for efficient spin–orbit torques," APL Mater. **9**(6), 060901 (2021).

[8] H. Park, K. Jeong, I. Maeng, K.I. Sim, S. Pathak, J. Kim, S.-B. Hong, T.S. Jung, C. Kang, J.H. Kim, J. Hong, and M.-H. Cho, "Enhanced Spin-to-Charge Conversion Efficiency in Ultrathin Bi $_2$ Se $_3$ Observed by Spintronic Terahertz Spectroscopy," ACS Appl. Mater. Interfaces **13**(19), 23153–23160 (2021).

[9] J.-C. Rojas-Sánchez, S. Oyarzún, Y. Fu, A. Marty, C. Vergnaud, S. Gambarelli, L. Vila, M. Jamet, Y. Ohtsubo, A. Taleb-Ibrahimi, P. Le Fèvre, F. Bertran, N. Reyren, J.-M. George, and A. Fert, "Spin to Charge Conversion at Room Temperature by Spin Pumping into a New Type of Topological Insulator: α -Sn Films," Phys. Rev. Lett. **116**(9), 096602 (2016).

[10] M. Dc, R. Grassi, J.Y. Chen, M. Jamali, D. Reifsnyder Hickey, D. Zhang, Z. Zhao, H. Li, P. Quarterman, Y. Lv, M. Li, A. Manchon, K.A. Mkhoyan, T. Low, and J.P. Wang, "Room-temperature high spin–orbit torque due to quantum confinement in sputtered BixSe(1–x) films," Nat. Mater. **17**(9), 800–807 (2018).

[11] N.H.D. Khang, Y. Ueda, and P.N. Hai, "A conductive topological insulator with large spin Hall effect for ultralow power spin–orbit torque switching," Nat. Mater. **17**(9), 808–813 (2018).

[12] T. Fan, N.H.D. Khang, T. Shirokura, H.H. Huy, and P.N. Hai, "Low power spin–orbit torque switching in sputtered BiSb topological insulator/perpendicularly magnetized CoPt/MgO multilayers on oxidized Si substrate," Appl. Phys. Lett. **119**(8), 082403 (2021).

[13] T. Manoj, Z. Wen, J. Uzuhashi, T. Ohkubo, H. Sukegawa, C. Murapaka, B. York, X. Liu, Q. Le, and S. Mitani, "Spin–Orbit Torque Modulated by Interface Chemistry in Topological BiSb/NiFe Bilayers with Titanium Insertion," ACS Appl. Electron. Mater. **6**(6), 4269–4276 (2024).

[14] H. Nguyen, D. Khang, S. Nakano, T. Shirokura, and P.N. Hai, "Ultralow power spin – orbit torque magnetization switching induced by a non - epitaxial topological insulator on Si substrates," Sci. Rep., 1–12 (2020).

[15] Z. Chi, Y.C. Lau, X. Xu, T. Ohkubo, K. Hono, and M. Hayashi, "The spin Hall effect of Bi-Sb alloys driven by thermally excited Dirac-like electrons," Sci. Adv. **6**(10), 1–10 (2020).

[16] A.M.S. M. M. Otrokov, I. I. Klimovskikh, F. Calleja, J.H.D. O. Vilkov, A. G. Rybkin, D. Estyunin, S. Mu, H.O. A. L. Vázquez de Parga, R. Miranda, and A.A. F. Guinea, J. I. Cerdá, E. V. Chulkov, "Crystal growth and characterization of topological insulator BiSb thin 5 6 films by sputtering deposition on sapphire substrates," (111), 0–13 (2018).

[17] J. Sasaki, H.H. Huy, N.H.D. Khang, P.N. Hai, Q. Le, B. York, X. Liu, S. Le, C. Hwang, M. Ho, and H. Takano, "Improvement of the Effective Spin Hall Angle by Inserting an Interfacial Layer in Sputtered BiSb Topological Insulator (Bottom)/Ferromagnet with In-Plane Magnetization," IEEE Trans. Magn. **58**(4), 2021–2024 (2022).

[18] H.H. Huy, Z. Ruixian, T. Shirokura, S. Takahashi, Y. Hirayama, and P.N. Hai, "Integration of BiSb topological insulator and CoFeB/MgO with perpendicular magnetic anisotropy using an oxide interfacial layer for ultralow power SOT-MRAM cache memory," IEEE Trans. Magn. **PP**, 1 (2023).

[19] C.-Z. Chang, P. Wei, and J.S. Moodera, "Breaking time reversal symmetry in topological insulators," MRS Bull. **39**(10), 867–872 (2014).

[20] Z. Ruixian, H.H. Huy, T. Shirokura, P.N. Hai, Q. Le, B. York, C. Hwang, X. Liu, M. Gribelyuk, X. Xu, S. Le, M. Maeda, T. Fan, Y. Tao, and H. Takano, "High spin Hall angle in BiSb topological insulator and perpendicularly magnetized CoFeB/MgO multilayers with metallic interfacial layers," Appl. Phys. Lett. **124**(7), 072402 (2024).

[21] S. Barua, and K.P. Rajeev, "Status of surface conduction in topological insulators," AIP Adv. **4**(1), 017135 (2014).

[22] Y. Ueda, N.H. Duy Khang, K. Yao, and P.N. Hai, "Epitaxial growth and characterization of Bi1-xSbx spin Hall thin films on GaAs(111)A substrates," Appl. Phys. Lett. **110**(6), 062401 (2017).
[23] S. Goel, N.H.D. Khang, Y. Osada, L.D. Anh, P.N. Hai, and M. Tanaka, "Room-temperature spin injection from a ferromagnetic semiconductor," Sci. Rep. **13**(1), 2181 (2023).
[24] H.H. Huy, J. Sasaki, N.H.D. Khang, S. Namba, P.N. Hai, Q. Le, B. York, C. Hwang, X. Liu, M. Gribelyuk, X. Xu, S. Le, M. Ho, and H. Takano, "Large inverse spin Hall effect in BiSb topological insulator for 4 Tb/in2 magnetic recording technology," Appl. Phys. Lett. **122**(5), 052401 (2023).
[25] K. Sriram, J. Pala, B. Paikaray, A. Haldar, and C. Murapaka, "Effect of seed layer thickness on the Ta crystalline phase and spin Hall angle," Nanoscale **13**(47), 19985–19992 (2021).
[26] A. Kumar, R. Bansal, S. Chaudhary, and P.K. Muduli, "Large spin current generation by the spin Hall effect in mixed crystalline phase Ta thin films," Phys. Rev. B **98**(10), 104403 (2018).
[27] I.M. Miron, K. Garello, G. Gaudin, P.-J. Zermatten, M.V. Costache, S. Auffret, S. Bandiera, B. Rodmacq, A. Schuhl, and P. Gambardella, "Perpendicular switching of a single ferromagnetic layer induced by in-plane current injection," Nature **476**(7359), 189–193 (2011).
[28] K. Sriram, R. Mondal, J. Pradhan, A. Haldar, and C. Murapaka, "Structural Phase Engineering of (α + β)-W for a Large Spin Hall Angle and Spin Diffusion Length," J. Phys. Chem. C **127**(46), 22704–22712 (2023).
[29] V.P. Amin, J. Zemen, and M.D. Stiles, "Interface-Generated Spin Currents," Phys. Rev. Lett. **121**(13), 136805 (2018).
[30] J. Song, C. He, T. Scheike, Z. Wen, H. Sukegawa, T. Ohkubo, Y. Nozaki, and S. Mitani, "Charge-to-spin conversion in fully epitaxial Ru/Cu hybrid nanolayers with interface control," Nanotechnology **34**(36), 365704 (2023).
[31] N.H.D. Khang, S. Nakano, T. Shirokura, Y. Miyamoto, and P.N. Hai, "Ultralow power spin–orbit torque magnetization switching induced by a non-epitaxial topological insulator on Si substrates," Sci. Rep. **10**(1), 12185 (2020).
[32] T. Fan, N. Huynh, D. Khang, S. Nakano, and P.N. Hai, "Ultrahigh efficient spin orbit torque magnetization switching in fully sputtered topological insulator and ferromagnet multilayers," Sci. Rep., 1–8 (2022).
[33] Q. Le, B.R. York, C. Hwang, X. Liu, L. Xu, S. Le, M. Maeda, T. Fan, Y. Tao, H. Takano, M. Liu, Z. Ruixian, S. Namba, and P. Nam Hai, "Thermal reliability and spin Hall angle of highly textured and epitaxial $Bi_{0.9}$ $Sb_{0.1}$ (012) topological insulator," Jpn. J. Appl. Phys. **64**(4), 043001 (2025).